

Generalized Ghost Dark Energy with Non-Linear Interaction

E. Ebrahimi^{1,2} *, H. Golchin¹ †, A. Mehrabi³ ‡ and S. M. S. Movahed^{4,5} §

¹*Department of Physics, Shahid Bahonar University, PO Box 76175, Kerman, Iran*

²*Research Institute for Astronomy and Astrophysics of Maragha (RIAAM), Maragha, Iran*

³*Department of Physics, Bu-Ali Sina University, Hamedan 65178, 016016, Iran*

⁴*Department of Physics, Shahid Beheshti university, G.C., Evin, Tehran 19839, Iran*

⁵*School of Physics, Institute for Research in Fundamental Sciences,
(IPM), P. O. Box 19395-5531, Tehran, Iran*

In this paper we investigate ghost dark energy model in the presence of non-linear interaction between dark energy and dark matter. The functional form of dark energy density in the generalized ghost dark energy (GGDE) model is $\rho_D \equiv f(H, H^2)$ with coefficient of H^2 represented by ζ and the model contains three free parameters as Ω_D, ζ and b^2 (the coupling coefficient of interactions). We propose three kinds of non-linear interaction terms and discuss the behavior of equation of state, deceleration and dark energy density parameters of the model. We also find the squared sound speed and search for signs of stability of the model. To compare the interacting GGDE model with observational data sets, we use more recent observational outcomes, namely SNIa, gamma-ray bursts, baryonic acoustic oscillation and the most relevant CMB parameters including, the position of acoustic peaks, shift parameters and redshift to recombination. For GGDE with the first non-linear interaction, the joint analysis indicates that $\Omega_D = 0.7009_{-0.0077}^{+0.0077}$, $b^2 = 0.171_{-0.042}^{+0.042}$ and $\zeta = 0.116_{-0.098}^{+0.044}$ at 1 optimal variance error. For the second interaction, the best fit values at 1σ confidence are $\Omega_D = 0.6961_{-0.0084}^{+0.0084}$, $b^2 = 0.054_{-0.014}^{+0.011}$ and $\zeta \leq 0.0445$. According to combination of all observational data sets considered in this paper the best fit values for third non-linearly interacting model are $\Omega_D = 0.6947_{-0.0086}^{+0.0086}$, $b^2 = 0.0143_{-0.0054}^{+0.0032}$ and $\zeta \leq 0.0326$ at 1σ confidence interval. Finally we found that the presence of interaction is confirmed in mentioned models via current observational data sets.

I. INTRODUCTION

Accelerating expansion of the universe is a mysterious event in the modern cosmology. The most relevant observational results based on SNIa as robust standard candle around 1998 demonstrated

* ebrahimi@uk.ac.ir

† h.golchin@uk.ac.ir

‡ Mehrabi@basu.ac.ir

§ m.s.movahed@ipm.ir

that our universe is experiencing an accelerative phase of expansion at the late time [1–4]. After that, other observational data sets provided by cosmic microwave background (CMB) [5–8] and large scale structure as well as baryon acoustic oscillation [9–15] favored mentioned acceleration phase. On the other hand, there are many models to achieve the late time acceleration epoch for evolution of our universe. In a more general and famous approach, the responsible for mentioned phase is generically relegated to the influence of a strange form of energy which is the so-called dark energy (DE). The simplest candidate for this approach is cosmological constant [16–18]. Such proposal is noticeable in the case that the right underlying theory of gravity is supposed to be general relativity (GR). Moreover there are some approaches to modify gravity in cosmological scales, in order to include the late time accelerating epoch [19–22]. Dynamical models of dark energy (models with time varying equation of state parameter) are also allowed from theoretical point of view, such models are supported by observational evidences. An incomplete list of examples includes time varying cosmological constant[23], quintessence[24–28], phantom fields [29–34], holographic dark energy which originate from quantum gravity approach[35–40], age graphic dark energy [41–43] and so on. An interesting problem which potentially can be resolved in dynamical approach is the so-called “coincidence problem”, which simply asks “why dark energy component becomes dominant at present time?”. It is also worth to mention that the acceleration problem can be addressed in the framework of modified gravity [44] (and references therein).

Ghost dark energy (GDE), is another dynamical DE model introduced in [45, 46]. GDE is based on the Veneziano ghost field which has already been introduced to solve the $U1$ problem in QCD theory [47–51]. In a Minkowskian spacetime there is not any observable consequence from the ghost field but turning into a dynamical spacetime the ghost field affects the vacuum energy density.

In the lowest level, ghost dark energy contribution to the vacuum energy density can be taken as $\Lambda_{QCD}^3 H$, where H is the Hubble parameter and Λ_{QCD}^3 is QCD mass scale [46]. In [45, 52], authors showed that this contribution is enough to drive an acceleration in the cosmic background. Considering the values $\Lambda_{QCD} \sim 100 MeV$ and $H \sim 10^{-33} eV$ one obtains $\Lambda_{QCD}^3 H \sim (3 \times 10^{-3} eV)$ which solve the fine tuning problem[46]. Another interesting feature of this model is that there is no need to introduce new degrees of freedom since GDE is totally embedded in the known physics. Different features of GDE is extensively studied [53–59].

The influence of the ghost field to the vacuum energy density was reconsidered in reference [60]. They found that, there exists a second order term proportional to H^2 which can contribute to the vacuum energy density. Accordingly, the ghost dark energy density can be redefined as

$\rho_D = \alpha H + \beta H^2$ [60] where α and β are constants. The dark energy model which is based on this relation is called generalized ghost dark energy (GGDE). According to previous results represented in [60, 61] concerning GGDE model, the second order term (βH^2) has opposite dynamical influence with respect to the linear term (αH). Subsequently, one can expect that some problems with GDE will be removed in the generalization approach.

As mentioned before, cosmological constant or in brief Λ is one of the first candidates can explain dynamical evolution of the universe with accelerating expansion rate. In the standard model of cosmology entitled Λ CDM, dark sectors namely, DE (Λ) and dark matter (DM) evolve separately and do not interact. However, because of the unclear nature of both DE and DM, it is possible to consider interaction between the dark sectors in the universe and there is not any theoretical reason against such an interaction [24]. Interacting models are also capable to solve the coincidence problem. There also exists observational evidences which support the interacting models [62, 63].

Considering an interaction between DE and DM, there will arise a simple question that what is the form of the interaction term? Phenomenologically one can choose the interaction terms as a linear combination of ρ_D and ρ_m at the simplest level. It has been also shown that a product coupling (an interaction term proportional to the product of ρ_D , ρ_m and their summation), is consistent with observations [64].

Our aim in this paper is to consider a new form of non-linear interaction term seeking better agreement with observations and improving model defects such as stability. Observational consistency check has vital role not only for either to accept or to rule out underlying model but also for doing reliable comparison between different proposed theoretical models for describing the universe. Therefore, in this paper we put observational constraints on the free parameters of our interacting dynamical dark energy model regarding to observations related to background evolution. The most recent data for SNIa Joint Light-curve Analysis (JLA) sample will be considered. Also to make more completeness of objects at high redshift, Gamma-Ray-Bursts (GRBs) will be taken into account. Various measurements for determining the Baryon Acoustic Oscillation (BAO) including Sloan Digital Sky Survey (SDSS), Baryon Oscillation Spectroscopic Survey (BOSS), WiggleZ survey and 6dFGS survey are included. The major contribution of DE is at late epoch so here we consider the position of sound horizon, shift parameter and redshift of recombination from CMB observation, nevertheless it is possible to use CMB power spectrum to do much more completed evaluation. Finally, the joint analysis of all mentioned observational data to determine the best fit values for model free parameters has been done. As an other interesting investigation, one can

explore the influence of GDE on the large scale structure in the universe, which will be done in separate work.

This paper is outlined as follows. In the next section, we review linearly interacting and non-interacting GGDE models in a flat universe. Section III is devoted to extension from linear to non-linear interaction. In section IV we will rely on the most recent observational data to check the consistency of our model. To this end, following indicators will be taken into account: SNIa, Gamma Ray Bursts as a complementary part to the SNIa observations, Baryonic Acoustic oscillation and CMB observational quantities including shift parameter, location of the first peak and redshift to recombinations. We summarize our results in section V.

II. GGDE MODEL WITH A GENERAL INTERACTION TERM IN FLAT UNIVERSE

In this section we review GGDE model in general case. We will focus on the absence and presence of an interaction term between dark sectors of our universe. In this paper we limit ourself to influence of GGDE on the background evolution of universe and for the sake of clarity, as a beginning task we start with the Friedmann equation in a flat universe:

$$H^2 = \frac{8\pi G}{3} (\rho_r + \rho_m + \rho_D), \quad (1)$$

where ρ_r , ρ_m and ρ_D are the energy densities of radiation, pressure-less matter (including dark and baryonic) and dark energy, respectively. According to the GGDE model [60], the energy density of the dark energy defined by:

$$\rho_D = \alpha H + \beta H^2. \quad (2)$$

The dimensionless energy density of various components are:

$$\begin{aligned} \Omega_m &\equiv \frac{\rho_m}{\rho_{cr}} = \frac{8\pi G \rho_m}{3H^2}, \\ \Omega_D &\equiv \frac{\rho_D}{\rho_{cr}} = \frac{8\pi G(\alpha + \beta H)}{3H}, \\ \Omega_r &\equiv \frac{\rho_r}{\rho_{cr}} = \frac{8\pi G \rho_r}{3H^2}. \end{aligned} \quad (3)$$

where $\rho_{cr} = 3H^2/(8\pi G)$, so the first Friedmann equation can be written as $\Omega_r + \Omega_m + \Omega_D = 1$. Here we assume that a coupling term (Q) exists between dark energy and dark matter components. So the energy conservation equations read as:

$$\dot{\rho}_m + 3H\rho_m = Q, \quad (4)$$

$$\begin{aligned}\dot{\rho}_D + 3H\rho_D(1 + w_D) &= -Q, \\ \dot{\rho}_r + 3H\rho_r(1 + w_r) &= 0,\end{aligned}\tag{5}$$

where $w_D = \frac{P_D}{\rho_D}$ and $w_r = 1/3$. Summing above equations one finds the total energy density conservation equation: $\dot{\rho} + 3H(\rho + P) = 0$, where $\rho = \rho_r + \rho_m + \rho_D$ and the total pressure equals $P = P_r + P_D$. Taking the time derivative of (1) we find:

$$\dot{H} = -4\pi G\rho_D[y(1 + w_r) + 1 + u + w_D],\tag{6}$$

where $y = \rho_r/\rho_D$ and $u = \rho_m/\rho_D$. Differentiating (2) with respect to time and also replacing \dot{H} from (6), we reach the following relation

$$\dot{\rho}_D = -4\pi G\rho_D [y(1 + w_r) + 1 + u + w_D] (\alpha + 2\beta H),\tag{7}$$

so the conservation equation for DE (5), takes to the form

$$4\pi G u(\alpha + 2\beta H) - \frac{Q}{\rho_D} = (1 + w_D)[3H - 4\pi G(\alpha + 2\beta H)] - 4\pi Gy(1 + w_r)(\alpha + 2\beta H),\tag{8}$$

now introducing $\zeta \equiv \frac{8\pi G\beta}{3}$ and using the following relation

$$\frac{4\pi G}{3H}(\alpha + 2\beta H) = \frac{\Omega_D + \zeta}{2},\tag{9}$$

which is obtained from Ω_D in (3), it is possible to rewrite (8) as

$$u(\Omega_D + \zeta) - \frac{2Q}{3H\rho_D} = (1 + w_D)(2 - \Omega_D - \zeta) - y(1 + w_r)(\Omega_D + \zeta),\tag{10}$$

finally, noticing that $u = \frac{\Omega_m}{\Omega_D} = \frac{1}{\Omega_D} - 1$, the equation of state parameter w_D can be obtained as

$$\begin{aligned}w_D &= \frac{\zeta - \Omega_D - Q'\Omega_D - \Omega_r\Omega_D - \zeta\Omega_r + y(1 + w_r)(\Omega_D + \zeta)\Omega_D}{\Omega_D(2 - \Omega_D - \zeta)}, \\ Q' &= \frac{2Q}{3H\rho_D}.\end{aligned}\tag{11}$$

Now let us turn to the deceleration parameter which is defined in terms of scale factor a , as:

$$q = -\frac{a\ddot{a}}{\dot{a}^2} = -1 - \frac{\dot{H}}{H^2},\tag{12}$$

substituting \dot{H} from (6) and using the definition of Ω_D in (3), one can find

$$q = -1 + \frac{3}{2}\Omega_D [y(1 + w_r) + 1 + u + w_D].\tag{13}$$

By using the relation $\dot{\Omega}_D = H \frac{d\Omega_D}{d \ln a}$ one obtains the evolution of DE density parameter as $\frac{d\Omega_D}{d \ln a} = -\frac{8\pi G\alpha}{3H} \frac{\dot{H}}{H^2}$, noting (9), the evolution of Ω_D can be written as:

$$\frac{d\Omega_D}{d \ln a} = \frac{4\pi G\alpha}{H^2(\alpha + \beta H)} [y(1 + w_r) + 1 + u + w_D]. \quad (14)$$

Since we are interested in late time universe, the contribution of radiation is negligible. In this case, the above equation can be written as:

$$\frac{d\Omega_D}{d \ln a} = \frac{3}{2} (\Omega_D - \zeta)(1 + w_D \Omega_D). \quad (15)$$

Hereafter we consider $\Omega_r \rightarrow 0$ in all relevant equations, however for observational consideration, where the radiation has important contribution we will keep radiation density in relevant equations. Till now, we have shown the results in terms of a general form Q for interaction between DE and DM. To test the validity of the above results, we find the cosmological parameters w_D and q for some definite interactions. In the case of non-interacting model, setting $Q = Q' = 0$ in (11), (13); we find

$$w_D = \frac{\zeta - \Omega_D}{\Omega_D(2 - \Omega_D - \zeta)}, \quad q = \frac{1}{2} + \frac{3}{2} \frac{\zeta - \Omega_D}{2 - \zeta - \Omega_D}, \quad (16)$$

which are in agreement with the respective relations obtained in [61]. Another model for interaction is $Q = 3b^2 H(\rho_m + \rho_D) = 3b^2 H \rho_D(1 + u)$. This interaction is linear in terms of ρ , with a coupling constant b^2 . In this case one finds that $Q' = \frac{2b^2}{\Omega_D}$. Substituting this value to (11) and (13) leads to:

$$w_D = \frac{\zeta - \Omega_D - 2b^2}{\Omega_D(2 - \Omega_D - \zeta)}, \quad (17)$$

$$q = \frac{1}{2} + \frac{3}{2} \frac{\zeta - \Omega_D - 2b^2}{2 - \zeta - \Omega_D}, \quad (18)$$

and the evolution equation for energy density of DE is given by:

$$\frac{d\Omega_D}{d \ln a} = 3\Omega_D \left[\frac{1 - \Omega_D}{2 - \Omega_D - \zeta} \left(1 + \frac{2b^2}{\Omega_D} - \frac{\zeta}{\Omega_D} \right) - \frac{b^2}{\Omega_D} \right], \quad (19)$$

which are the same as the results in [61], [65]. In the next section we will consider some new non-linear functional forms for interaction between dark matter and dark energy.

III. NON-LINEAR INTERACTING GGDE MODEL IN FLAT UNIVERSE

As already mentioned, the main purpose of this paper is to examine the impact of non-linear interaction terms on the background of cosmic dynamics. In choosing the form of non-linear

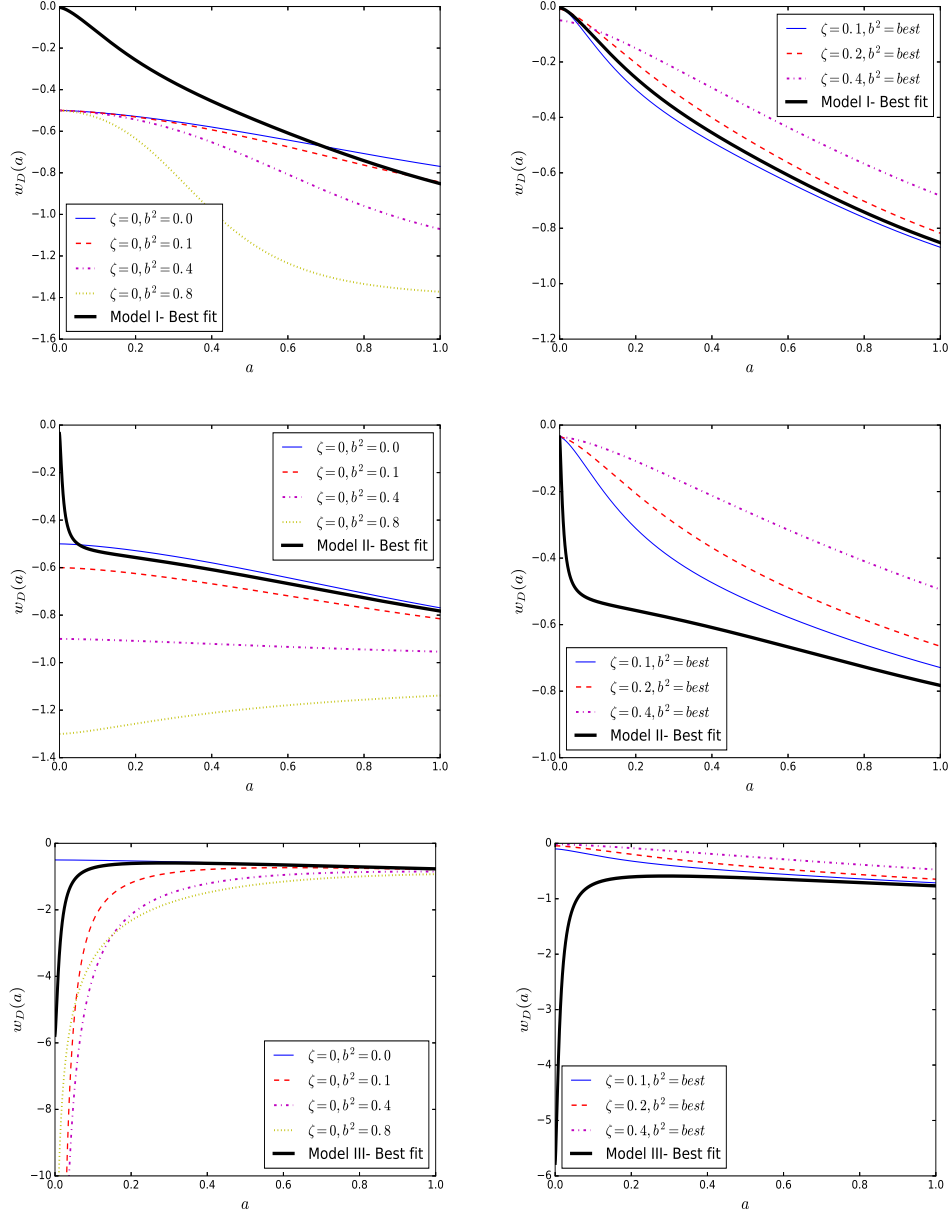


FIG. 1: The evolution of w_D as a function of scale factor for three models explained in the text. Left panels are devoted to $\zeta = 0$, while right panels correspond to best fit value for b^2 based on joint analysis of SNIa+GRBs+BAO+CMB. Here we consider scale factor at present time as $a_0 = 1$. The value of Ω_D at the present time is 0.70. In all plots the dark solid line corresponds to the best fit values determined by joint analysis. For the first model $\Omega_D = 0.7009^{+0.0077}_{-0.0077}$, $b^2 = 0.171^{+0.042}_{-0.042}$ and $\zeta = 0.116^{+0.044}_{-0.098}$. For the second model $\Omega_D = 0.6961^{+0.0084}_{-0.0084}$, $b^2 = 0.054^{+0.011}_{-0.014}$ and $\zeta \leq 0.0445$ and for the third model $\Omega_D = 0.6947^{+0.0086}_{-0.0086}$, $b^2 = 0.0143^{+0.0032}_{-0.0054}$ and $\zeta \leq 0.0326$.

interaction terms, we follow the prescription presented in [66]. The closed form of the interaction which includes a large variety of choices is

$$Q = 3Hb^2 \rho_m^p \rho_D^s \rho^r, \quad (20)$$

where $\rho = \rho_m + \rho_D$ and b^2 is coupling constant factor also p , s and r are integer numbers and one can deduce from the dimensional analysis that they should satisfy $p + s + r = 1$. In the following we choose three non-linear interactions and investigate their properties and features.

A. Model I

In this model we consider following non-linear interaction form

$$Q = 3b^2 H \frac{\rho_D^3}{\rho^2}, \quad (21)$$

for this interaction, noticing (11) one finds that $Q' = \frac{2b^2 \rho_D^2}{\rho^2}$ and considering the fact that $\rho = \rho_m + \rho_D$, it can be rewritten as $Q' = 2b^2 \Omega_D^2$. By inserting this relation to (11) and (13) we find

$$w_D = \frac{\zeta - \Omega_D - 2b^2 \Omega_D^3}{\Omega_D(2 - \Omega_D - \zeta)}, \quad (22)$$

$$q = \frac{1}{2} + \frac{3}{2} \frac{\zeta - \Omega_D - 2b^2 \Omega_D^3}{2 - \zeta - \Omega_D}. \quad (23)$$

It turns out that the above relations reduce to the corresponding expressions of non-interacting model (16) when $b = 0$. In Fig.(1) we have depicted the evolution of w_D as a function of scale factor for various values of the free parameters for this model. It is also clear from Fig. (1) that at late time, for some values of the free parameters, we get $w_D < -1$, which show a phantom like behavior of this interacting GGDE model. Fig. (2) indicates the deceleration parameter as a function of scale factor for various choices of ζ and b^2 parameters. Increasing the value of b^2 causes to decreasing q and getting the negative value at earlier time while according to right panel of Fig.(2), higher values of ζ resulting the higher values of decelerating parameter. In order to discuss about the fate of the universe filled with DM and GGDE components we should consider the effective equation of state parameter:

$$w_{eff} = \frac{P}{\rho}. \quad (24)$$

Taking $P_m = 0$, it can be found that $w_{eff} = \Omega_D w_D$. Fig.(3) represents w_{eff} as a function of scale factor. Our results demonstrate that $w_{eff} \rightarrow -1$ at future implying that the universe will end with a big rip. It can be seen from Fig.(3) that the universe enters a acceleration phase earlier for larger

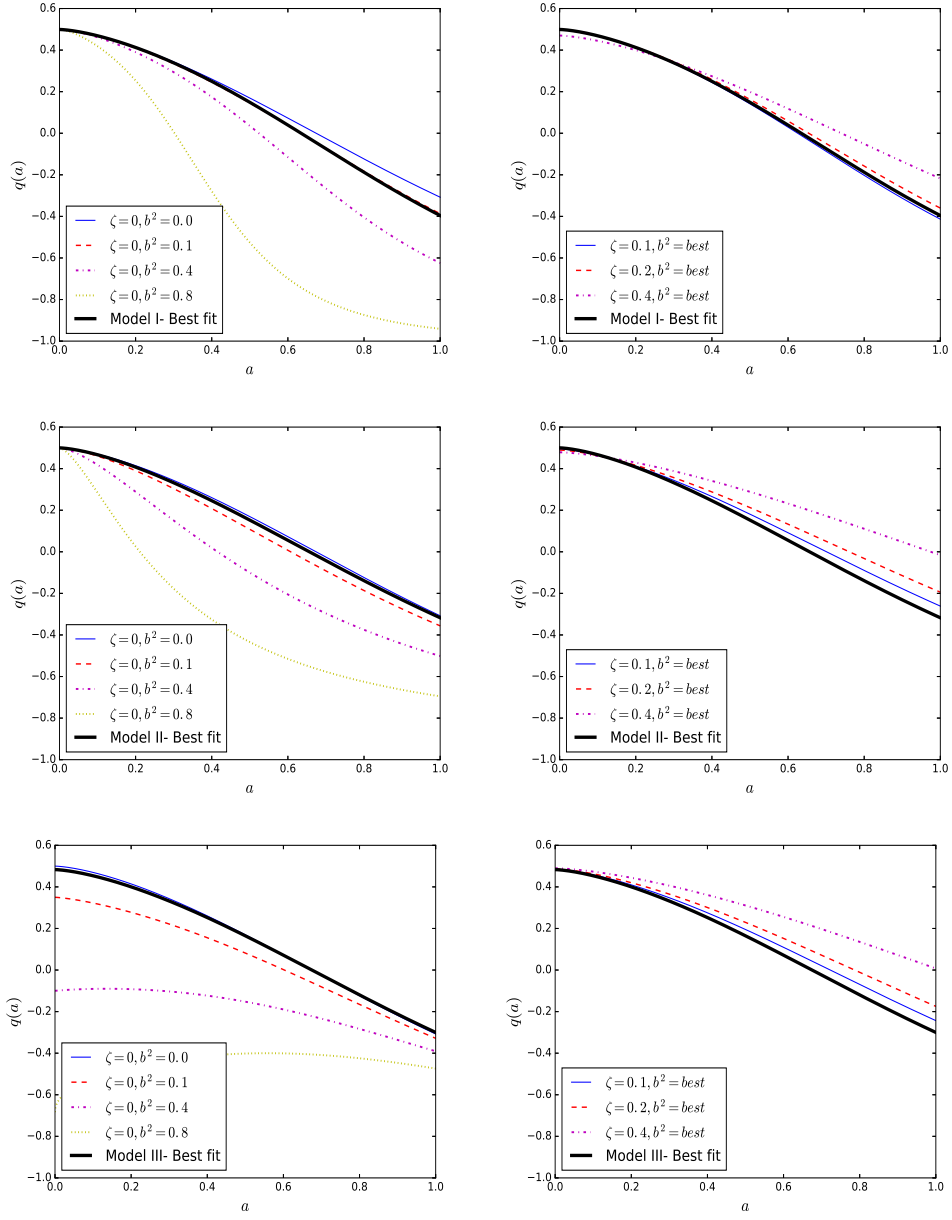


FIG. 2: The evolution of q as a function of scale factor for three models explained in the text. The rest information is the same as that of mentioned in Fig. 1.

values of b . In this case the evolution of DE density parameter can be computed using (14), the result is

$$\frac{d\Omega_D}{d \ln a} = \frac{3(\zeta - \Omega_D)(-1 + \Omega_D + b^2\Omega_D^3)}{2 - \Omega_D - \zeta}. \quad (25)$$

The evolution of DE density parameter versus a is depicted in Fig.(4). In the left part of this

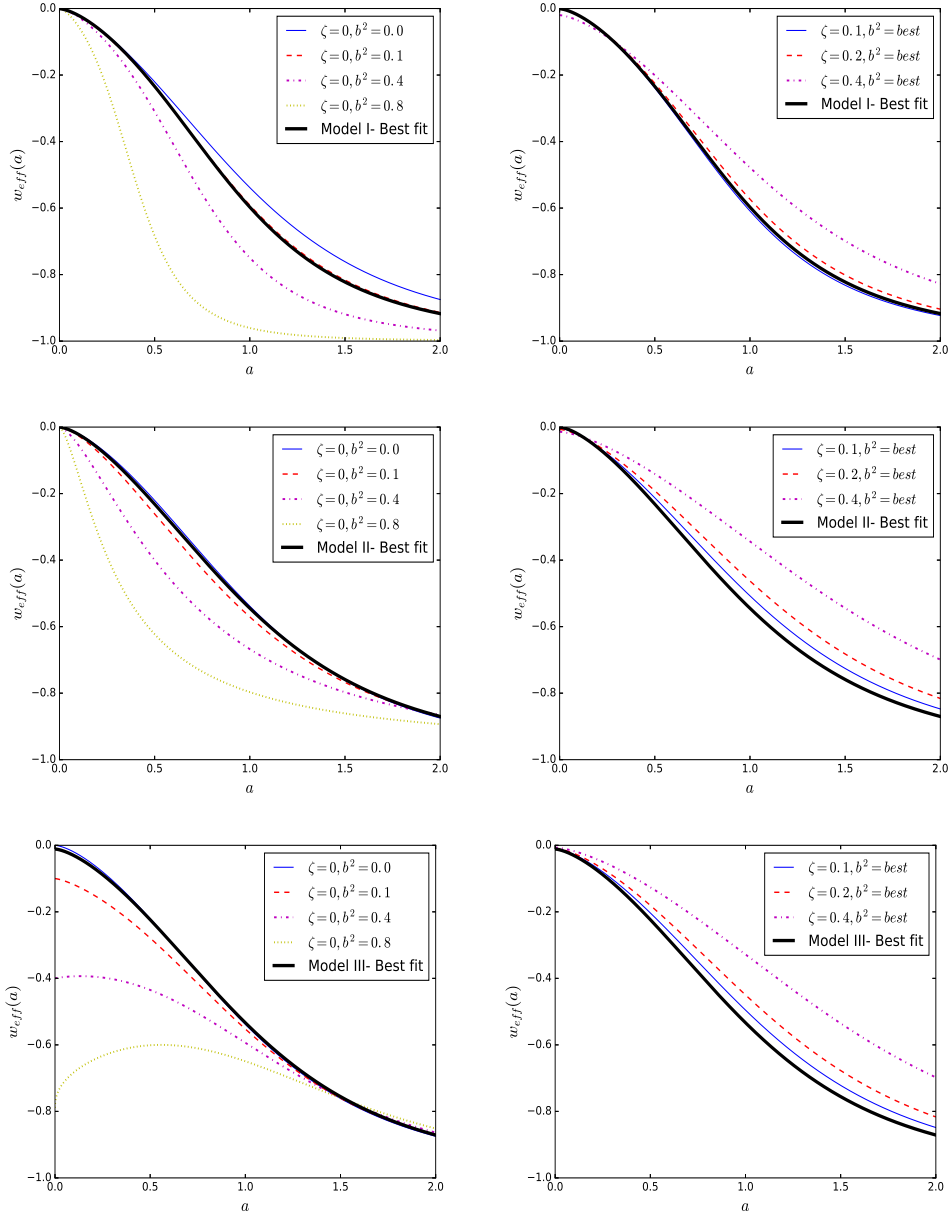


FIG. 3: The evolution of w_{eff} as a function of scale factor for three models explained in the text. The rest information is the same as that of mentioned in Fig. 1.

figure, we turned to the impact of the coupling constant b on the density parameter evolution. This figure shows that for larger values of b the evolution of Ω_D will be flatter. In the right panel of Fig.(4), evolution of Ω_D is plotted for different choices of ζ and best value for b^2 (see next section). This figure reveals that the main advantages of the squared term in the dark energy density happens in early stages of the universe. This result was expected because the second order term is very small at late epochs (due to smallness of H at late time). So it seems that the second

term just can affect the late time acceleration problem through its primary effects on the cosmic dynamics in earlier stages.

Currently our universe is in dark energy dominated phase, so any successful model must be able to result in a late time stable universe in the dark energy dominated phase. In order to consider the stability issue of a dark energy model we should discuss a covariant perturbation theory in an expanding background. However in this step we do not follow such a process. In fact, here we are interested to do a simple analysis to see if the universe shows signs of stability in the DE dominated phase. With a simple Newtonian analysis one finds that the factor which has signals about instability against small adiabatic perturbations in an expanding background is the squared sound speed $v_s^2 = \frac{dP}{d\rho}$. When $v_s^2 < 0$, the perturbations can grow and makes the background unstable while for $v_s^2 > 0$ the perturbations propagate oscillatory and the background will be stable against linear adiabatic perturbations. The way we use squared sound speed here is that we search for epochs with positive v_s^2 because we need a late time stable DE dominated universe. Here we look for impacts of the non-linear interaction terms to see if it leaves any chance for a late time positive $v_s^2 > 0$. Using

$$v_s^2 = \frac{dp}{d\rho} = \frac{\dot{p}}{\dot{\rho}}, \quad (26)$$

and taking into account the cosmic dynamic equations with non-linear interactions, after a little algebra one can find the squared sound speed as

$$v_s^2 = \frac{(\Omega_D - 1)(\Omega_D - \zeta)}{(\Omega_D - 2 + \zeta)^2} + \frac{\Omega_D^2(\Omega_D\zeta + 2\Omega_D - 6\zeta + 3\zeta^2)}{(\Omega_D - 2 + \zeta)^2} b^2. \quad (27)$$

In Fig.(5), v_s^2 is drawn versus a . From the left part it is obvious that for this class of interaction, v_s^2 with suitable choice of coupling constant b , is capable to get positive values at the late times and this leaves a chance for stable dark energy dominated universe which favored by observations. Fig.(5) also indicates that for larger values of b , v_s^2 will transits earlier to positive domain. It is worth mentioning that GDE in non-interacting and linearly interacting cases suffers from the negativity of v_s^2 at the late times [65] and this is a direct consequence of this form of non-linear interaction term. The right part of Fig.(5) reveals that for larger values of ζ , v_s^2 will enter to the positive domain later. The evolution of scale factor as a function of time can be computed using Eq. (9) as follows:

$$\int_{a_0}^a (\Omega_D - \zeta) \frac{da'}{a'} = \int_{t_0}^t \frac{8\pi G\alpha}{3} dt' = B(t - t_0) \quad (28)$$

where $B \equiv \frac{8\pi G\alpha}{3}$. Fig. (6) illustrates the behavior of scale factor as a function of time. The plot shows that this model can explain the late time accelerating expansion of the universe.

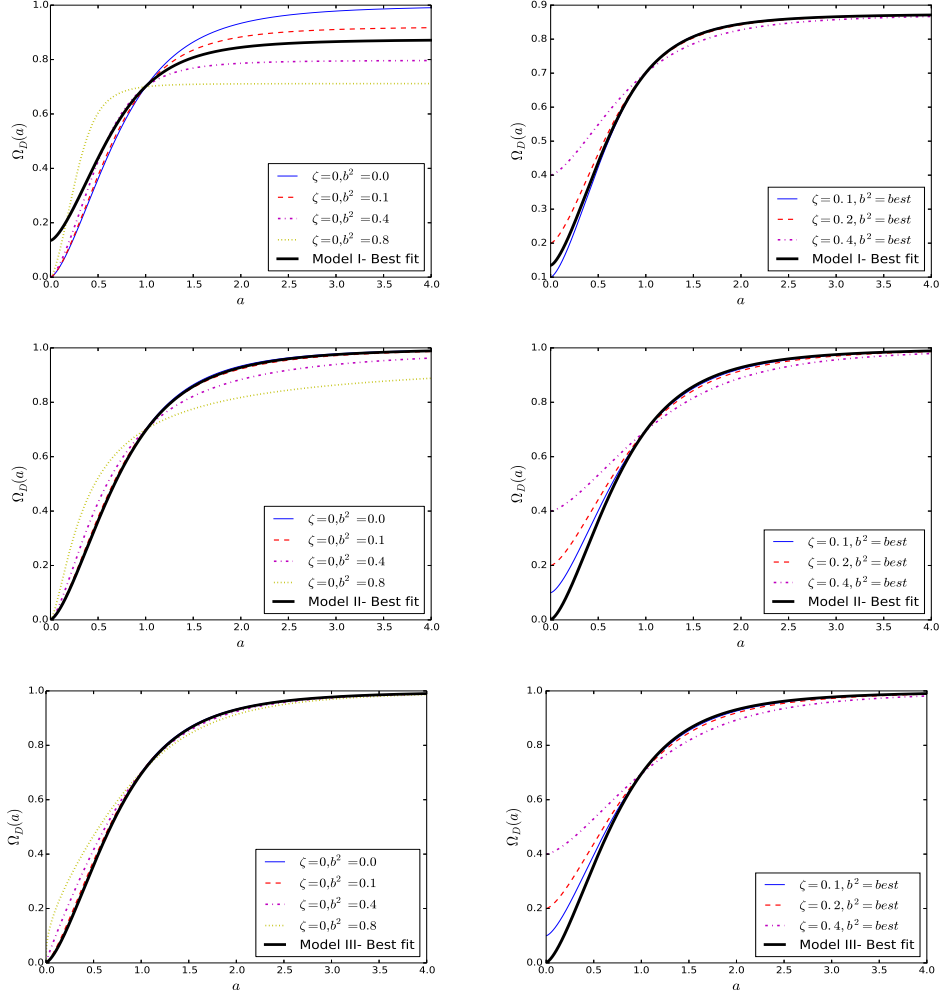


FIG. 4: The evolution of Ω_D as a function of scale factor for three models explained in the text. The rest information is the same as that of mentioned in Fig. 1.

B. Model II

In this model we consider the following form for non-linear interaction term

$$Q = 3b^2 H \frac{\rho_D \rho_m}{\rho}. \quad (29)$$

In this case, one finds that $Q' = \frac{2b^2 \rho_m}{\rho} = 2b^2 \Omega_m$ consequently, we can rewrite the equation of state and deceleration parameters as

$$w_D = \frac{\zeta - \Omega_D - 2b^2 \Omega_D (1 - \Omega_D)}{\Omega_D (2 - \Omega_D - \zeta)}, \quad (30)$$

$$q = \frac{1}{2} + \frac{3}{2} \frac{\zeta - \Omega_D - 2b^2 \Omega_D (1 - \Omega_D)}{2 - \zeta - \Omega_D}. \quad (31)$$

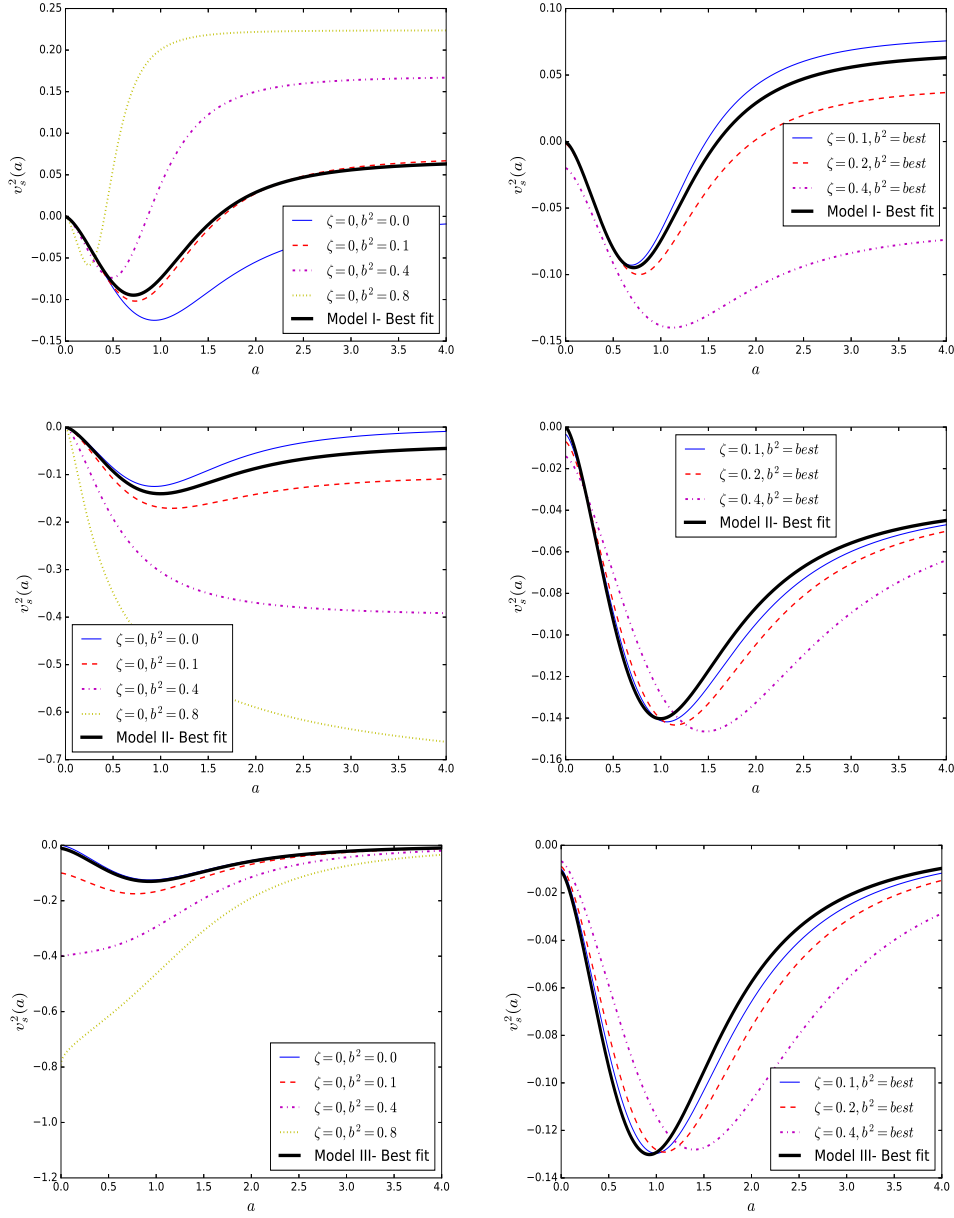


FIG. 5: The evolution of v_s^2 as a function of scale factor for three models explained in the text. The rest information is the same as that of mentioned in Fig. 1.

It is easy to see that these relations in the late and early time limits approach to the non-interacting case, however they differ from non-interacting case in middle stages of evolution. It is also worth to mention that in this case the phantom divide can not be crossed. To make more obvious the mentioned behavior, we have plotted the relevant parameters.

In Fig.(1) we found that the evolution of w_D versus scale factor. Fig.(2) indicates the deceleration parameter as function of scale factor for various choices of ζ and b^2 parameters. Increasing the

value of b^2 causes to decreasing q and getting the negative value at earlier times while according to the right panel of Fig.(2), larger values of ζ leads to the larger deceleration parameters. Note that to ensure $q < 0$ at the present time ($a = 1$), we should set $\zeta < 0.4$. This theoretical constraint is consistent to the other observational constraints (the next section).

Fig.(3) illustrates w_{eff} as a function of scale factor. Our results demonstrate that $w_{eff} \rightarrow -1$ at future implying that the universe will end with a big rip as the previous case. It can be seen from Fig.(3) that w_{eff} gets more negative values by increasing the coupling b^2 . One can also find the evolution of DE density parameter for this case as

$$\frac{d\Omega_D}{d \ln a} = \frac{3(\zeta - \Omega_D)(1 - \Omega_D)(b^2\Omega_D - 1)}{2 - \Omega_D - \zeta}. \quad (32)$$

The left part of Fig.(4) corresponds to the impact of the coupling constant b^2 on the density parameter evolution. This figure shows that larger values of b^2 , extend the dominant era of Ω_D . In right panel of this figure, the evolution of Ω_D is plotted for different choices of ζ .

In this case the squared sound speed can be obtained as:

$$v_s^2 = \frac{(\Omega_D - 1)(\Omega_D - \zeta)}{(\Omega_D - 2 + \zeta)^2} - \frac{\Omega_D^3 + (\zeta - 2)\Omega_D^2 + (2\zeta^2 - 5\zeta + 2)\Omega_D - \zeta^2 + 2\zeta}{(\Omega_D - 2 + \zeta)^2} b^2. \quad (33)$$

Plotting v_s^2 versus a in Fig.(5) reveals that the squared sound speed is always negative for different choices of constants implying that in present case, a late time stable GGDE dominated phase is not recovered. It is also easy to see that by increasing b , the squared sound speed takes larger negative values in contrast with the previous case.

C. Model III

The functional form of non-linear interaction for this model is considered as

$$Q = 3b^2 H \frac{\rho_m^2}{\rho}. \quad (34)$$

Doing the same steps for this interaction, one finds that $Q' = 2b^2 \frac{\rho_m^2}{\rho\rho_D} = 2b^2 \frac{\Omega_m^2}{\Omega_D}$, and the EoS and deceleration parameters as

$$w_D = \frac{\zeta - \Omega_D - 2b^2(1 - \Omega_D)^2}{\Omega_D(2 - \Omega_D - \zeta)} \quad (35)$$

$$q = \frac{1}{2} + \frac{3}{2} \frac{\zeta - \Omega_D - 2b^2(1 - \Omega_D)^2}{2 - \zeta - \Omega_D}. \quad (36)$$

In this case the dark energy density parameter evolves as

$$\frac{d\Omega_D}{d \ln a} = \frac{3(\zeta - \Omega_D)(\Omega_D - 1)(b^2\Omega_D + 1 - b^2)}{2 - \Omega_D - \zeta}. \quad (37)$$

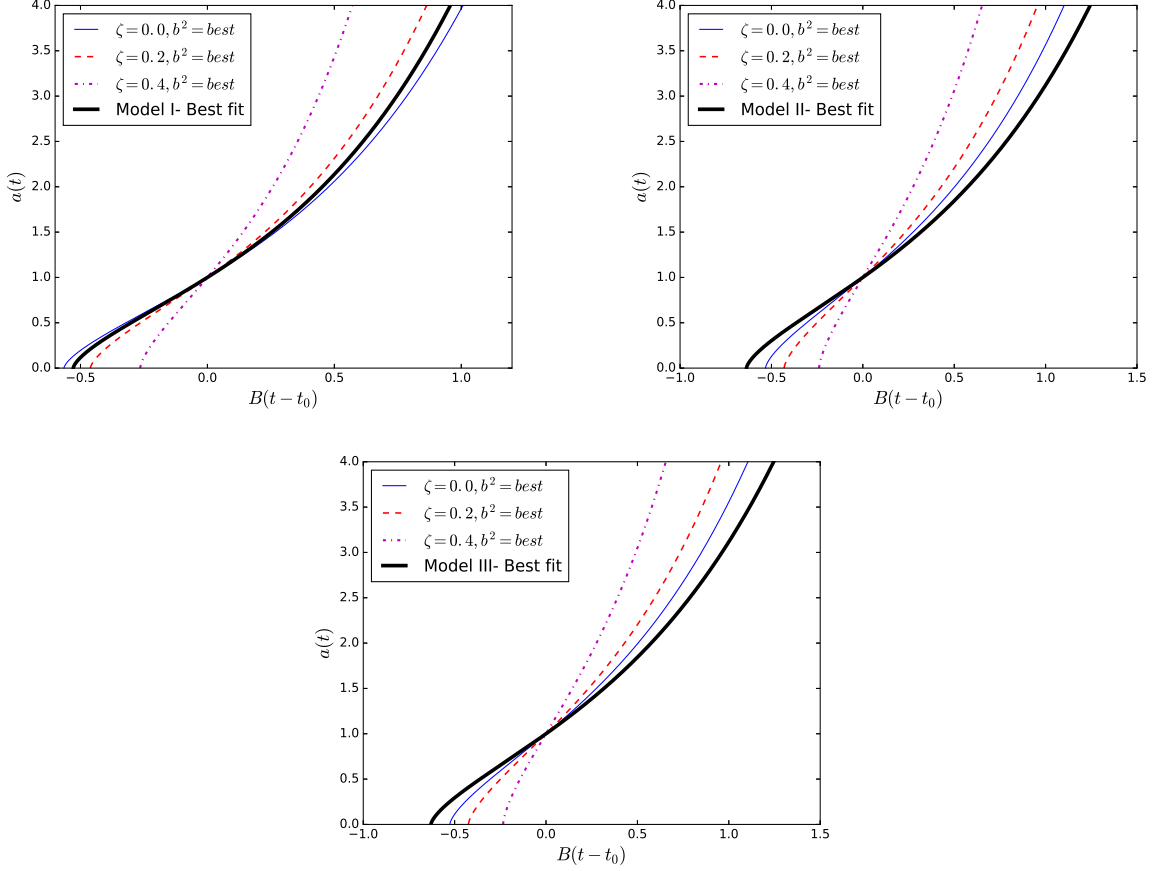


FIG. 6: The evolution of scale factor as a function of time. Here $B \equiv \frac{8\pi G\alpha}{3}$, the value of Ω_D at the present time is 0.70 and b^2 has been fixed according to its best values determined by joint analysis of SNIa+GRBs+BAO+CMB. In all plots the dark solid line corresponds to the best fit values determined by joint analysis. For the first model $\Omega_D = 0.7009^{+0.0077}_{-0.0077}$, $b^2 = 0.171^{+0.042}_{-0.042}$ and $\zeta = 0.116^{+0.044}_{-0.098}$. For the second model $\Omega_D = 0.6961^{+0.0084}_{-0.0084}$, $b^2 = 0.054^{+0.011}_{-0.014}$ and $\zeta \leq 0.0445$ and for the third model $\Omega_D = 0.6947^{+0.0086}_{-0.0086}$, $b^2 = 0.0143^{+0.0032}_{-0.0054}$ and $\zeta \leq 0.0326$.

The behavior of equation of state, w_D , deceleration parameter, q , effective equation of state, w_{eff} and energy density of DE have been plotted in Figs. (1), (2), (3) and (4), respectively. Finally the squared sound speed for this case reads

$$v_s^2 = \frac{(\Omega_D - 1)(\Omega_D - \zeta)}{(\Omega_D - 2 + \zeta)^2} + \frac{(\Omega_D - 1) [\Omega_D^2 + (\zeta - 3)\Omega_D + (2\zeta - 5)\zeta + 4]}{(\Omega_D - 2 + \zeta)^2} b^2. \quad (38)$$

Fig.(5) shows that in this case v_s^2 can not get positive values but approaches the border line at the future. The model with smaller value of b will approaches the border line earlier. Finally, the behavior of scale factor as a function of time is represented in Fig.(6). This plot shows that the model in principle, can explain the late accelerating expansion of the universe.

Till now, we investigated the overall behavior of three non-linear interacting models. Here,

we summarize and compare the behavior of w_D , q , w_{eff} , Ω_d and v_s^2 for these three models. The behavior of w_D in model I and model II as a function of scale factor for different values of free parameters namely ζ and b^2 are almost similar while for third model, the value of w_D at very early times goes to large negative values. The deceleration parameter q in the third model is very sensitive to b^2 , it also get different values when $a \rightarrow 0$, while for the first and second models the value of q at early stages is almost similar for different free parameters. The behavior of w_{eff} and Ω_D as a function of scale factor are somehow similar to the situation dealing with q . From the v_s^2 point of view, model I presents positive values for some values of free parameters, while for models II and III the squared sound speed takes negative values at least for accepted values of free parameters. In the next section we are going to carry out the comparison between results given by our models and that of given directly from observation.

IV. OBSERVATIONAL CONSISTENCY CHECK

In this section, we rely on the most recent observational data to check the consistency of generalized ghost dark energy model accompanied by non-linear interactions between DM and DE. This approach enables us to put observational constraints on the free parameters of our model. The following observables for examination of the nature of dark energy can be used:

- I) Expansion history of the Universe
- II) Changing the evolution of gravitational potentials, causing to ISW effect
- III) Cross-correlation of CMB and large scale structures
- IV) Growth of structures
- V) Weak lensing

In this paper we limit ourselves on almost evolution expansion indicators such as distance modulus of Supernovae Type Ia and the Gamma-Ray Bursts (GRBs), Baryon acoustic oscillations (BAO) and CMB including the position of first peak, shift parameter and redshift of recombination. Throughout this paper we have supposed that our Universe is flat, so $\Omega_{tot} = \Omega_m + \Omega_b + \Omega_r + \Omega_D = 1$, where Ω_m, Ω_b denote the density parameters of dark matter and baryonic matter respectively. Energy density of radiation and baryonic matter are fixed by other relevant observations. For convenient, we indicate free parameters by $\Theta : \{\Omega_D, \zeta, b^2\}$. The expected priors on these parameters are listed in Table I. Radiation density is fixed to $\Omega_r = 2.469 \times 10^{-5} h^{-2} (1.6903)$ [67]. The baryonic density is set to $\Omega_b h^2 = 0.02222 \pm 0.00023$ [68]

Parameter	Prior	Shape of PDF
Ω_{tot}	1.000	Fixed
ζ	[0.050 – 0.020]	Top-Hat
H_0	[40.0 – 100.0]	Top-Hat
Ω_D	[0.0 – 1.0]	Top-Hat
b^2	[0.0 – 1.0]	Top-Hat

TABLE I: Priors on free parameter space, used in the observational constraints analysis in this paper.

A. Supernovae Ia

In this paper we consider constraints on model parameters coming from SNIa observations. For comparison and also for the sake of complementarity, we used the latest Union2.1 compilation released by the Supernova Cosmology Project Collaboration consisting of 580 SN Ia data points [8, 69]. The systematic errors of the observed distance modulus is also considered [69, 70]. Observation of SNIa does not provide standard ruler but rather gives distance modulus. This quantity is defined by:

$$\mu(z; \{\Theta\}) \equiv m - M = 5 \log \left(\frac{d_L(z; \{\Theta\})}{Mpc} \right) + 25 \quad (39)$$

where m and M are apparent and absolute magnitude, respectively. For the spatially flat universe the luminosity distance defined in above equation reads as:

$$d_L(z) = \frac{c}{H_0} (1+z) \int_0^z \frac{dz'}{\mathcal{H}(z'; \{\Theta\})} \quad (40)$$

where $\mathcal{H} = H/H_0$. To compare the observational data and that of determined by our model, we apply the likelihood analysis. To this end, we use χ^2 which is defined as

$$\chi_{SNIa}^2 \equiv \Delta\mu^\dagger \cdot \mathcal{C}_{SNIa}^{-1} \cdot \Delta\mu \quad (41)$$

where $\Delta\mu \equiv \mu_{obs}(z) - \mu(z; \{\Theta\})$ and correlation information of SNIa data sets is encoded in covariance matrix, \mathcal{C}_{SNIa} . The observed distance moduli and the relevant covariance matrix can be found on the web site [71]. Here $\mu_{obs}(z)$ is observed distance modulus for a SNIa located at redshift z . Marginalizing over H_0 as a nuisance parameter yields [8, 72]

$$\chi_{SNIa}^2 = \mathcal{M}^\dagger \cdot \mathcal{C}_{SNIa}^{-1} \cdot \mathcal{M} + \mathcal{A}_{SNIa} + \mathcal{B}_{SNIa} \quad (42)$$

where $\mathcal{M}(z) \equiv \mu_{obs}(z) - 25 - 5 \log_{10}[H_0 d_L(z; \{\Theta\})/c]$, and

$$\mathcal{A}_{SNIa} \equiv - \frac{\left[\sum_{i,j} \mathcal{M}(z_i) \mathcal{C}_{SNIa}^{-1}(z_i, z_j) - \ln 10/5 \right]^2}{\sum_{i,j} \mathcal{C}_{SNIa}^{-1}(z_i, z_j)} \quad (43)$$

$$\mathcal{B}_{SNIa} \equiv -2 \ln \left(\frac{\ln 10}{5} \sqrt{\frac{2\pi}{\sum_{i,j} C_{SNIa}^{-1}(z_i, z_j)}}} \right) \quad (44)$$

In addition to SNIa standard candles, Gamma-Ray Bursts (GRBs) which are the most luminous astrophysical objects at high redshift [73–77] will also taken into account. The χ_{GRBs}^2 is given by [78]:

$$\chi_{GRBs}^2 = \sum_i \frac{\mathcal{M}^2(z_i)}{\sigma_i^2} + \mathcal{A}_{GRBs} + \mathcal{B}_{GRBs} \quad (45)$$

where

$$\mathcal{A}_{GRBs} \equiv - \frac{\left[\sum_i \frac{\mathcal{M}(z_i)}{\sigma_i^2} - \ln 10/5 \right]^2}{\sum_i \frac{1}{\sigma_i^2}} \quad (46)$$

$$\mathcal{B}_{GRBs} \equiv -2 \ln \left(\frac{\ln 10}{5} \sqrt{\frac{2\pi}{\sum_i \frac{1}{\sigma_i^2}}} \right) \quad (47)$$

B. Baryon acoustic oscillations

The footprint of oscillations in the baryon-photon plasma on the matter power spectrum is recognized by Baryon Acoustic Oscillation (BAO). The acoustic scale is so large therefore BAO are largely unaffected by nonlinear evolution. Usually, the BAO data is applied to measure both the angular diameter distance $D_A(z; \{\Theta\})$, and the expansion rate of the Universe $H(z; \{\Theta\})$ [8]:

$$D_V(z; \{\Theta\}) = \left[(1+z)^2 D_A^2(z; \{\Theta\}) \frac{cz}{H(z; \{\Theta\})} \right]^{1/3} \quad (48)$$

where $D_V(z; \{\Theta\})$ is volume-distance. The distance ratio is defined by

$$d(z; \{\Theta\}) \equiv \frac{r_s(z; \{\Theta\})}{D_V(z; \{\Theta\})} \quad (49)$$

here $r_s(z; \{\Theta\})$ is the comoving sound horizon. In order to take into account various aspects of BAO observations, we use six BAO indicators including Sloan Digital Sky Survey (SDSS) data release 7 (DR7) [79], SDSS-III Baryon Oscillation Spectroscopic Survey (BOSS) [80], WiggleZ survey [81] and 6dFGS survey [82]. These measurements include redshifts in the range $z \in [0.1, 0.7]$. Table II reports the observed value of mentioned parameters.

Redshift	Data Set	$r_s/D_V(z; \{\Theta\})$	Ref.
0.10	6dFGS	0.336 ± 0.015	[82]
0.35	SDSS-DR7-rec	0.113 ± 0.002	[79]
0.57	SDSS-DR9-rec	0.073 ± 0.001	[80]
0.44	WiggleZ	0.0916 ± 0.0071	[83]
0.60	WiggleZ	0.0726 ± 0.0034	[83]
0.73	WiggleZ	0.0592 ± 0.0032	[83]

TABLE II: Observed data for BAO [67].

The fisher information matrix is given by [67]

$$\mathcal{C}_{BAO}^{-1} = \begin{pmatrix} 4444.4 & 0 & 0 & 0 & 0 & 0 \\ 0 & 34.602 & 0 & 0 & 0 & 0 \\ 0 & 0 & 20.661157 & 0 & 0 & 0 \\ 0 & 0 & 0 & 24532.1 & -25137.7 & 12099.1 \\ 0 & 0 & 0 & -25137.7 & 134598.4 & -64783.9 \\ 0 & 0 & 0 & 12099.1 & -64783.9 & 128837.6 \end{pmatrix}. \quad (50)$$

Accordingly, χ_{BAO}^2 is written by

$$\chi_{BAO}^2 \equiv \Delta d^\dagger \cdot \mathcal{C}_{BAO}^{-1} \cdot \Delta d. \quad (51)$$

In above equation $\Delta d(z; \{\Theta\}) \equiv d_{obs}(z) - d(z; \{\Theta\})$, where \mathcal{C}_{BAO}^{-1} is given in (50) and $d_{obs}(z)$ is reported in table IV B. In the next subsection for sake of clarity, we will give proper explanation about the main constraints with CMB observations mainly affecting the background evolution.

C. CMB observations

The most popular quantities devoted to CMB power spectrum are the position of sound horizon in power spectrum (l_a), CMB shift parameter (R) and the redshift of recombination (z_*). The sound horizon angular scale at recombination in the flat Universe read as

$$l_a = \pi \frac{\int_0^{z_*} \frac{dz}{H(z; \{\Theta\})}}{r_s(z_*; \{\Theta\})}. \quad (52)$$

The CMB shift parameter represented by R is defined by

$$R(z_*; \{\Theta\}) = \sqrt{\Omega_m} \int_0^{z_*} \frac{dz}{\mathcal{H}(z; \{\Theta\})}. \quad (53)$$

here, the redshift at the recombination expresses as $z_* = 1048[1 + 0.00124(\Omega_b h^2)^{-0.738}(1 + g_1(\Omega_m h^2)^{g_2})]$. Where the relevant parameters g_1 and g_2 can be found in Ref. [84].

$$g_1 = \frac{0.0783 (\Omega_b h^2)^{-0.238}}{1 + 39.5 (\Omega_b h^2)^{0.763}}, \quad (54)$$

$$g_2 = \frac{0.560}{1 + 21.1 (\Omega_b h^2)^{1.81}}. \quad (55)$$

To consider the contribution of mentioned observational quantities, we use following likelihood function for CMB observation [67]:

$$\chi_{CMB}^2 = \Delta \mathcal{D}^\dagger \cdot \mathcal{C}_{CMB}^{-1} \cdot \Delta \mathcal{D}, \quad (56)$$

where $\Delta \mathcal{D} \equiv \mathcal{D}_{obs} - \mathcal{D}(\{\Theta\})$, in which \mathcal{D}_{obs} for the 9-year WMAP (WMAP9) observation with flat prior are [67]

$$\mathcal{D}_{obs} \equiv \begin{pmatrix} l_a \\ R \\ z_* \end{pmatrix} = \begin{pmatrix} 302.40 \\ 1.7246 \\ 1090.88 \end{pmatrix}, \quad (57)$$

and \mathcal{C}_{CMB} is as follows

$$\mathcal{C}_{CMB}^{-1} = \begin{pmatrix} 3.182 & 18.253 & -1.429 \\ 18.253 & 11887.879 & -193.808 \\ -1.429 & -193.808 & 4.556 \end{pmatrix}. \quad (58)$$

According to Planck TT+LowP data the most important parameters to use are [8]

$$\mathcal{D}_{obs} \equiv \begin{pmatrix} l_a \\ R \\ \Omega_b h^2 \end{pmatrix} = \begin{pmatrix} 301.76, \\ 1.7488 \\ 0.02228 \end{pmatrix}, \quad (59)$$

and \mathcal{C}_{CMB} is as follows

$$\mathcal{C}_{CMB} = \begin{pmatrix} 1 & 0.54 & -0.63 \\ 0.54 & 1 & -0.43 \\ -0.63 & -0.43 & 1 \end{pmatrix}. \quad (60)$$

In this paper we use the former observational quantities for CMB. Finally, we perform a MCMC analysis using joint likelihood of both standard rulers and standard candles. The combined chi-square function is:

$$\chi_{SGBC}^2 = \chi_{SN}^2 + \chi_{GRBs}^2 + \chi_{BAO}^2 + \chi_{CMB}^2. \quad (61)$$

The abbreviation (SGBC) stands in above equation is replaced by SNIa+GRBs+BAO+CMB. In the next subsection we will summarize the results achieved for best fit values of the free parameters and compare them.

D. Results

In the following, we present the observational constraints on the free parameters of ghost dark energy model with three interaction terms introduced in section III.

Model I: $Q = 3b^2 H \frac{\rho_D^3}{\rho^2}$

SNIa + GRBs observational constraint shows that $\Omega_D = 0.784_{-0.043}^{+0.058}$, $\zeta = 0.25 \pm 0.11$ and $b^2 < 0.146$ at 1σ confidence interval. The best fit values at 68% and 95% intervals for SNIa+GRBs are reported in Table III. Fig.7 also indicates the distance modulus for interacting GDE models. In this plot, we take the best values for free parameters fixed by SNIa+GRBs. In the upper left panel of Fig.8 the contour plot for the parameters of model I, confined by SNIa+GRBs observations is illustrated. Combining the other observational data sets, namely BAO and CMB with SNIa+GRBs observations results in $\Omega_D = 0.7009_{-0.0077}^{+0.0077}$, $\zeta = 0.116_{-0.098}^{+0.044}$ and $b^2 = 0.171_{-0.042}^{+0.042}$ at 1σ confidence interval. Table III reports the value at 68% and 95% optimal variance errors. Upper left panels of figures 9 and 10 illustrate the marginalized likelihood functions and contours for free parameter of first dark energy model using SNIa+GRBs+BAO and SNIa+GRBs+BAO+CMB respectively.

Parameters of model I	SNIa+GRBs	SNIa+GRBs+BAO	SGBC
Ω_D	$0.784_{-0.043-0.100}^{+0.058+0.088}$	$0.756_{-0.051-0.088}^{+0.051+0.084}$	$0.7009_{-0.0077-0.015}^{+0.0077+0.015}$
ζ	$0.25_{-0.11-0.25}^{+0.11+0.19}$	$0.23_{-0.15-0.23}^{+0.11+0.21}$	$0.116_{-0.098}^{+0.044} < 0.244$
b^2	$< 0.146 < 0.394$	$< 0.260 < 0.456$	$0.171_{-0.042-0.078}^{+0.042+0.075}$

TABLE III: Best fit values for non-linear interacting dark energy model I using SNIa+GRBs, SNIa+GRBs+BAO and joint combination of SNIa+GRBs+BAO+CMB (SGBC) at 68% and 95% confidence intervals.

Parameter of model II	SNIa+GRBs	SNIa+GRBs+BAO	SGBC
Ω_D	$0.775^{+0.061+0.100}_{-0.051-0.110}$	$0.772^{+0.063+0.100}_{-0.046-0.110}$	$0.6961^{+0.0084+0.0160}_{-0.0084-0.0170}$
ζ	$0.23^{+0.12+0.20}_{-0.15-0.23}$	$0.25^{+0.12+0.20}_{-0.12-0.24}$	$< 0.0445 < 0.0903$
b^2	$0.24^{+0.11+0.21}_{-0.15-0.24}$	$0.25^{+0.13}_{-0.18} < 0.459$	$0.054^{+0.011+0.026}_{-0.014-0.024}$

TABLE IV: Best fit values for non-linear interacting dark energy model II using SNIa+GRBs,SNIa+GRBs+BAO and joint combination of SNIa+GRBs+BAO+CMB (SGBC) at 68% and 95% confidence intervals.

Parameter of model III	SNIa+GRBs	SNIa+GRBs+BAO	SGBC
Ω_D	$0.813^{+0.054+0.085}_{-0.035-0.096}$	$0.814^{+0.045+0.077}_{-0.030-0.084}$	$0.6947^{+0.0086+0.0160}_{-0.0086-0.0180}$
ζ	$0.211^{+0.093}_{-0.160} < 0.424$	$0.22^{+0.11}_{-0.14} < 0.424$	$< 0.0326 < 0.0676$
b^2	$0.25^{+0.11+0.21}_{-0.13-0.21}$	$0.26^{+0.12+0.21}_{-0.12-0.22}$	$0.0143^{+0.0032+0.0100}_{-0.0054-0.0086}$

TABLE V: Best fit values for non-linear interacting dark energy model III using SNIa+GRBs, SNIa+GRBs+BAO and joint combination of SNIa+GRBs+BAO+CMB (SGBC) at 68% and 95% confidence intervals.

Model II: $Q = 3b^2 H \frac{\rho_D \rho_m}{\rho}$

For this model, SNIa+GRBs observations constrain the value of parameters as: $\Omega_D = 0.775^{+0.061}_{-0.051}$, $\zeta = 0.23^{+0.12}_{-0.15}$ and $b^2 = 0.24^{+0.11}_{-0.15}$ at 1σ confidence interval. The best fit values at 68% and 95% intervals for SNIa+ GRBs and their joint analysis are reported in table IV. Fig.7 also indicates the distance modulus for second interacting dark energy model. In the upper right panel of Fig.8 the

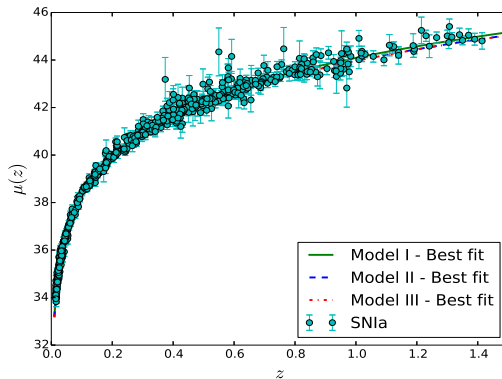


FIG. 7: Distance modulus as a function of redshift for model I, II and III. Here the value of Ω_D , ζ and b^2 take their best values according to SNIa+GRBs observational constraint.

contour plot for the model parameters confined by SNIa+GRBs observations is illustrated. Combining BAO and CMB observational data sets with SNIa+GRBs, results in $\Omega_D = 0.6961^{+0.0084}_{-0.0084}$, $\zeta < 0.0445$ and $b^2 = 0.054^{+0.011}_{-0.014}$ at 1σ confidence interval. Table IV reports the value at 68% and 95% levels. Upper right panels of Figs. 9 and 10 illustrate the marginalized likelihood functions and contours for free parameters of the second dark energy model.

Model III: $Q = 3b^2 H \frac{\rho_m^2}{\rho}$

For the third interacting dark energy model, SNIa+GRBs observations confine the value of parameters as: $\Omega_D = 0.813^{+0.054}_{-0.035}$, $\zeta = 0.211^{+0.093}_{-0.16}$ and $b^2 = 0.25^{+0.11}_{-0.13}$ at 1σ confidence interval. The best fit values at 68% and 95% intervals for SNIa+GRBs and their joint analysis are reported in table V. In addition, Fig. 7 indicates the distance modulus for this interacting dark energy model. In the bottom panel of Fig.8 the contour plot for the model parameters confined by SNIa+GRBs observation is illustrated. Combining the other observational data sets, namely BAO and CMB with SNIa+GRBs observations leads to $\Omega_D = 0.6947^{+0.0086}_{-0.0086}$, $\zeta < 0.0326$ and $b^2 = 0.0143^{+0.0032}_{-0.0054}$ at 1σ confidence interval. Table V reports these values at 68% and 95% levels. Bottom panels of Figs. 9 and 10 illustrate the marginalized likelihood functions and contours for free parameters of this model.

In order to give a quantitative and robust measure to compare three interacting dark energy models we must go beyond computing χ^2 and take into account the number of degrees of freedom (dof). Referring to the fact that higher degrees of freedom usually cause to more consistency of the model and observations, we use AIC [85] and BIC [86] criteria. AIC is defined by:

$$\text{AIC} = -2 \ln \mathcal{L}_{\max} + 2g, \quad (62)$$

Model	χ^2_{min}	AIC	BIC	χ^2_{min}/dof
I	576.0	586.0	608.3	0.894
II	579.3	589.3	611.6	0.899
III	581.2	591.2	613.5	0.902

TABLE VI: The minimum value of χ^2 , AIC and BIC criteria for our models.

and BIC [86] is given by:

$$\text{BIC} = -2 \ln \mathcal{L}_{\max} + g \ln N, \quad (63)$$

In the above equations, g is the number of free parameters and N is the number of observational data sets used for constraining. The relative form of mentioned criteria are in principle utilized, namely $\Delta\text{AIC} = \Delta\chi^2_{\min} + 2\Delta g$ and $\Delta\text{BIC} = \Delta\chi^2_{\min} + \Delta g \ln N$. The lower values of ΔAIC and ΔBIC , the more favored model by observational data sets. Regarding the capability of AIC and BIC measures, the former does not consider the number of observational data set, while the latter takes into accounts observations [87]. Since three models introduced in this paper have same degrees of freedom, therefore ΔAIC and ΔBIC don't make sense. The relevant results for our three cases are summarized in Tab.VI.

Finally, in order to compare three models of dark energy introduced in this paper, we indicate the behavior of Ω_D , q , v_s^2 , w_d and w_{eff} for the best fit values of free parameters as a function of scale factor in Fig.11. As indicated in this plot, from the view point of q and w_{eff} the three models are rather similar and they show the expected behavior of accelerating expansion of the universe. There is also some features that distinct these models, for instance Ω_D for model I takes non-zero value at very early universe while this quantity for model II and III goes to zero. The value of v_s^2 for first model takes positive value for $a > 1$ but for second and third models this quantity always remains in the negative domain. The w_D for third model goes to large negative values while for model I and II this quantity remains in interval $w_D \in [-1, 0]$.

The best values of parameters and their uncertainties have been shown in Tab.(VII), Tab.(VIII) and Tab.(IX) respectively.

V. SUMMARY AND CONCLUSION

Ghost dark energy (GDE) is one of interesting models that solves the recent acceleration problem. A great point about GDE is that this model is based on the Veneziano ghost field which

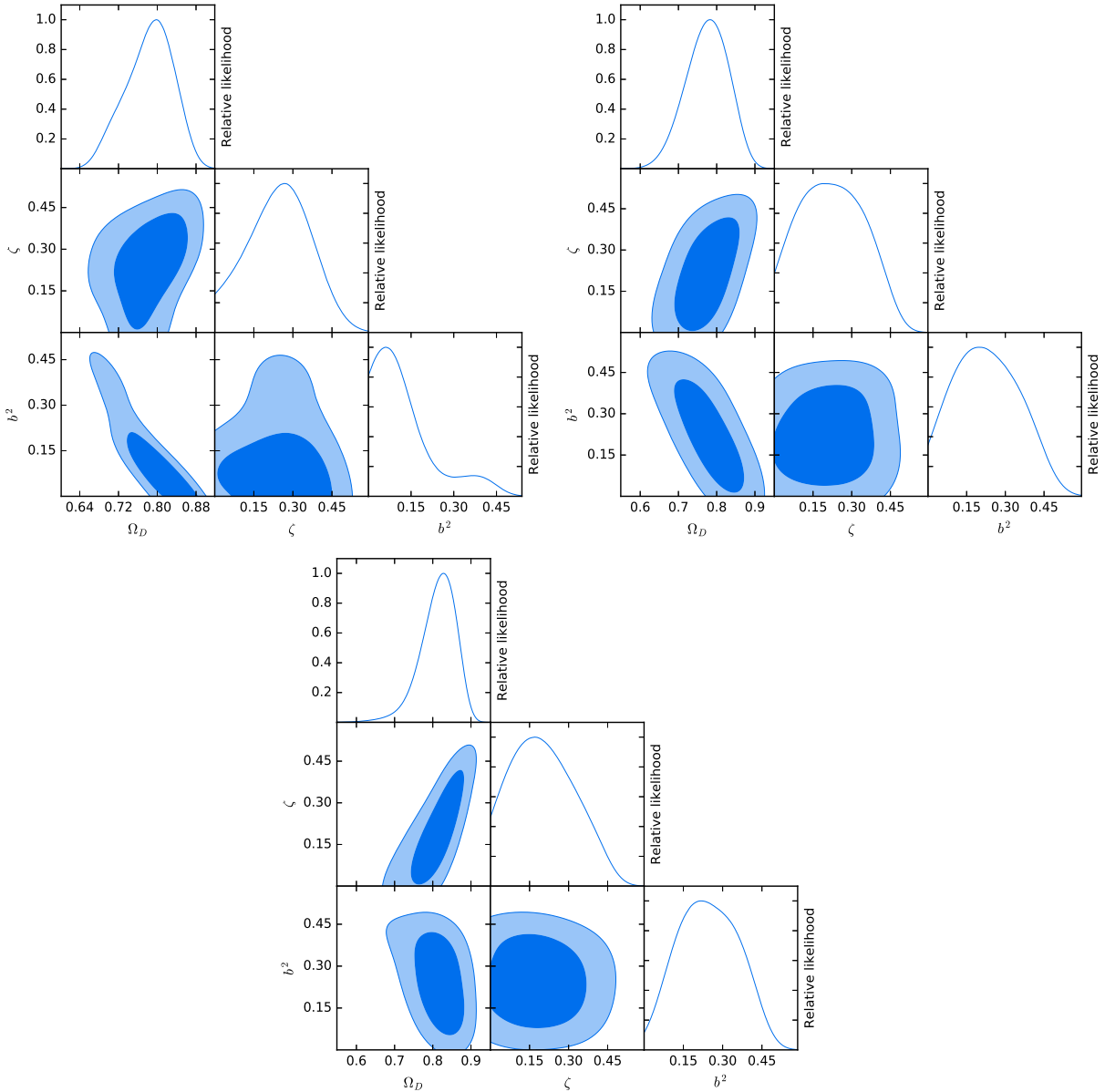


FIG. 8: Upper left panel corresponds to marginalized and contour plots of joint analysis base on SNIa+GRBs observations. The upper right panel shows the same for second model while the lower panel is devoted to model III of non-linear interacting dark energy.

has already presented in the literature and there is no need to introduce any additional degree of freedom in physics. This model also solves the coincidence problem [52]. However, GDE shows signs of instability (due to negativity of adiabatic squared sound speed v_s^2) in non-interacting and linear interacting domain. It is possible to redefine dark energy density candidate to the generalized ghost dark energy (GGDE) form as $\rho_D \equiv f(H, H^2)$ which the coefficient of H^2 is related to $\zeta = \frac{8\pi G\beta}{3}$. We also extended the interaction between DE and DM to non-linear regime seeking for

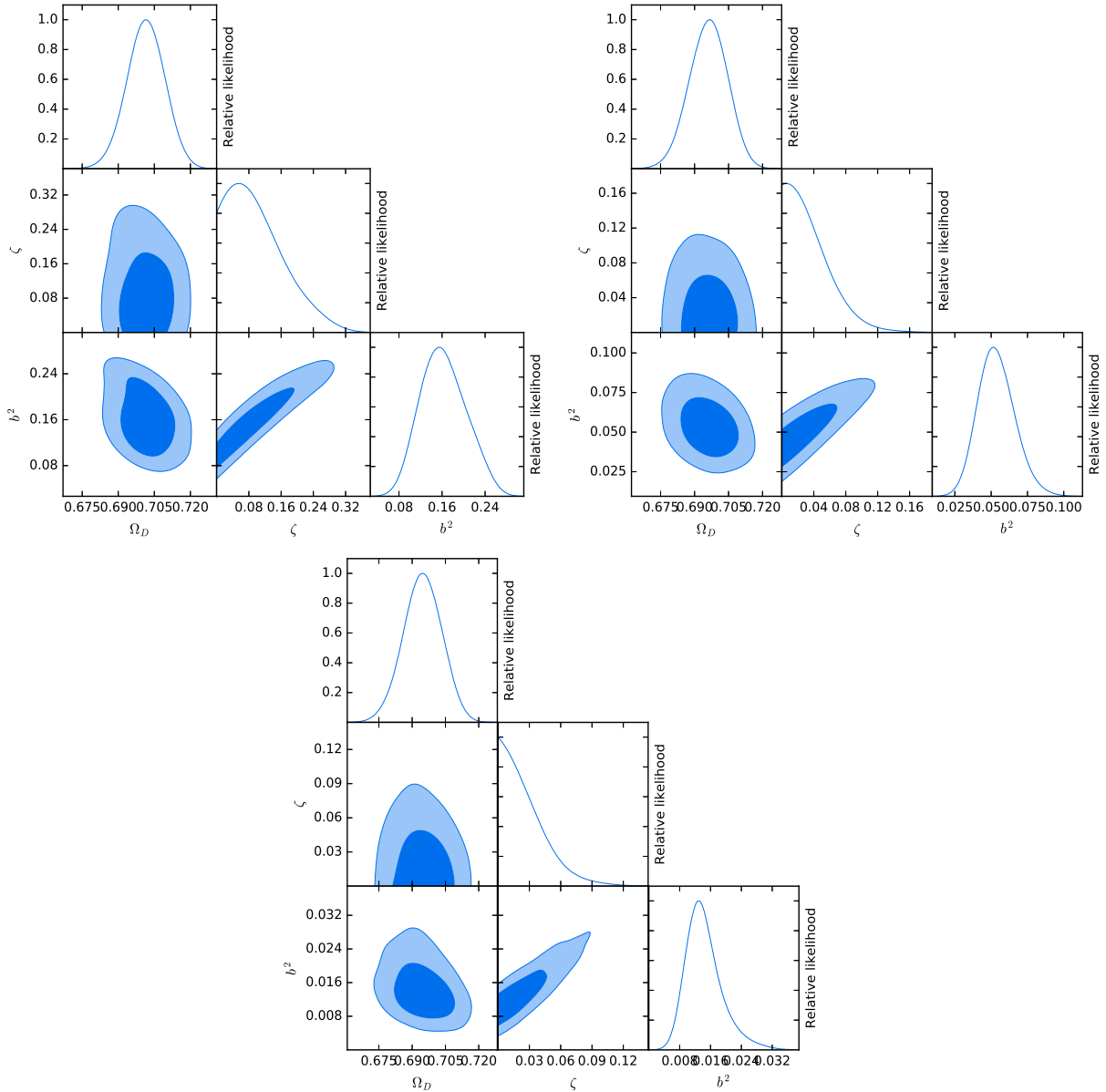


FIG. 9: Upper left panel corresponds to marginalized and contour plots of joint analysis base on SNIa+GRBs+BAO observations. The upper right panel shows the same for second model while the lower panel is devoted to model III of non-linear interacting dark energy.

better agreement with observations and improving the negativity of squared sound speed of the model.

To this end, we proposed three forms of non-linear interaction terms and investigated different features of these models. Generally, one can consider the functional form $Q \equiv f(H, \rho_m, \rho_D, \rho_{tot})$ for interaction between dark sectors of the universe with a coupling coefficient denoted by b^2 . We considered GGDE with non-linear interaction terms in the form $Q = 3b^2 H \rho_D^3 / \rho^2$, $Q = 3b^2 H \rho_D \rho_m / \rho$

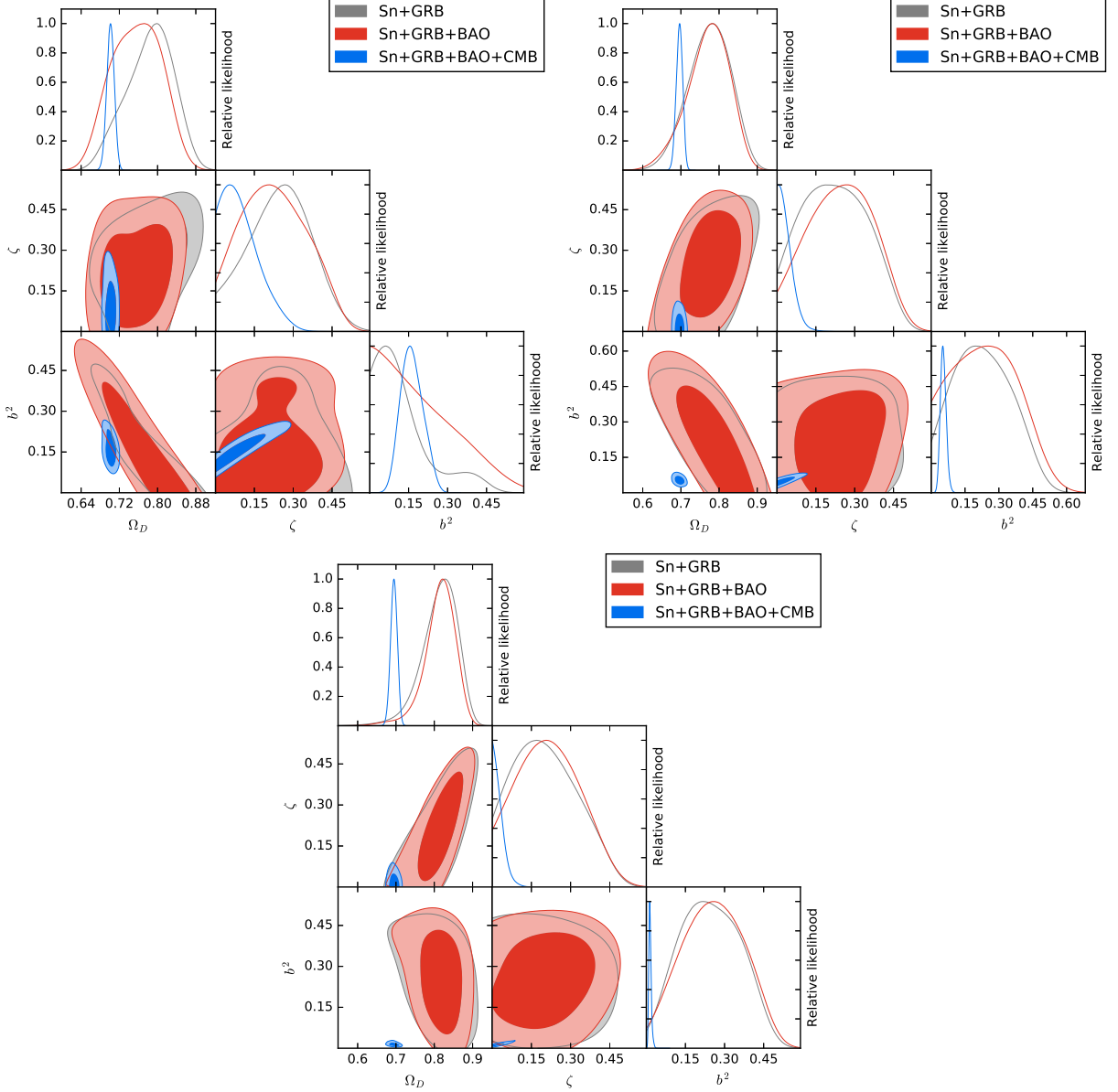


FIG. 10: Upper left panel corresponds to marginalized and contour plots of joint analysis base on SNIa+GRBs, SNIa+GRBs+BAO and SNIa+GRBs+BAO+CMB observations. The upper right panel shows the same for second model while the lower panel is devoted to model III of non-linear interacting dark energy.

and $Q = 3b^2 H \rho_m^2 / \rho$ as model I, II and III, respectively. If we suppose the universe is flat, the free parameters of the models are $\{\Omega_D, \zeta, b^2\}$.

We evaluated the behavior of $w_D(a)$, $q(a)$, $w_{eff}(a)$, $\Omega_D(a)$ and $v_s^2(a)$. As an interesting result we found that v_s^2 takes positive values at $a > 1$ for the best fit values of parameters of the model I (Fig.11), which is a sign of stability of this model. However the squared sound speed of models II, III remains negative. Considering the variations of q , w_{eff} (Fig.11), one can see that all models

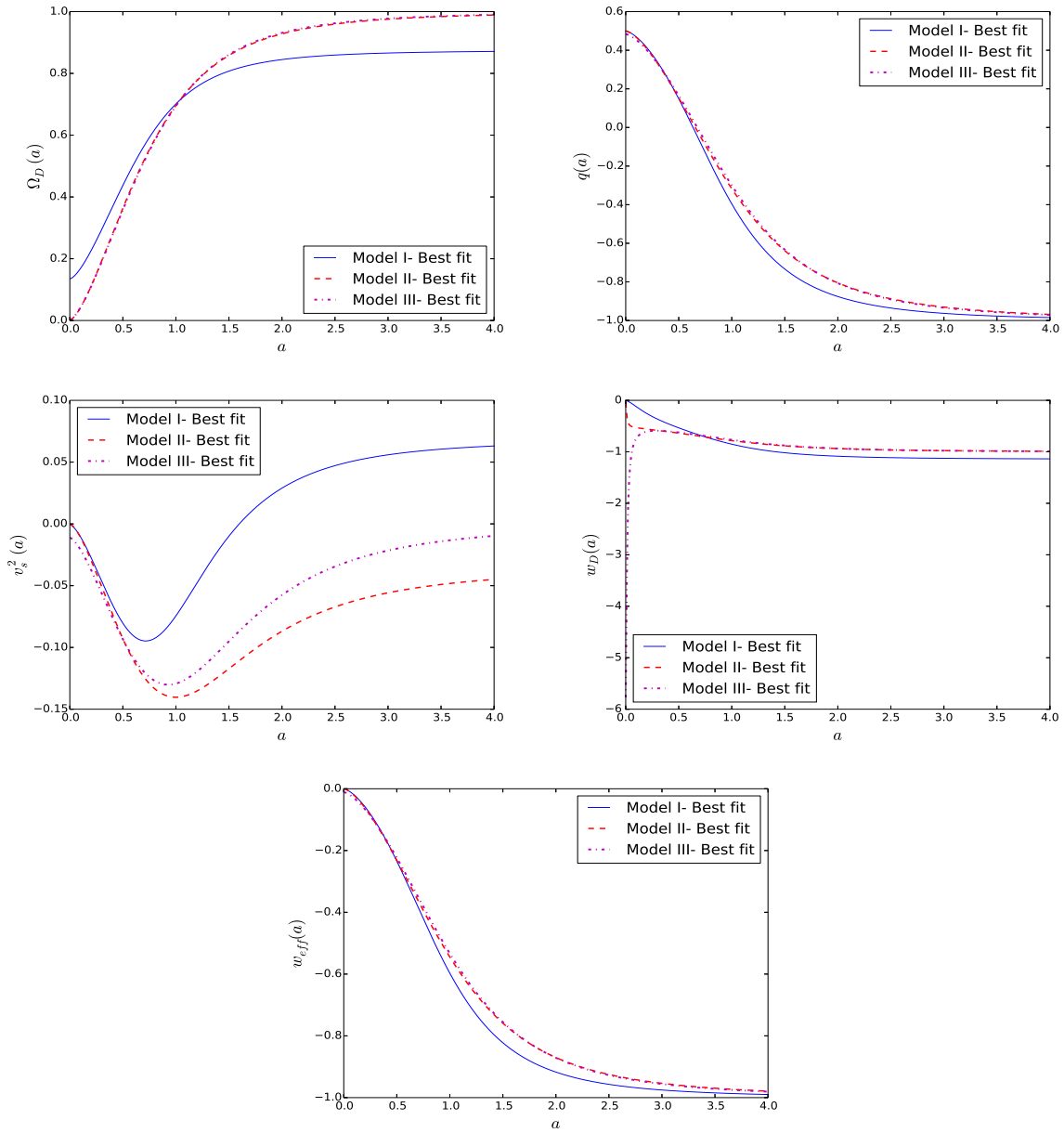


FIG. 11: The functional behavior of Ω_D , q , v_s^2 , w_d and w_{eff} for model I, II and III for the best fit value of free parameters. For the first model $\Omega_D = 0.7009^{+0.0077}_{-0.0077}$, $b^2 = 0.171^{+0.042}_{-0.042}$ and $\zeta = 0.116^{+0.044}_{-0.098}$. For the second model $\Omega_D = 0.6961^{+0.0084}_{-0.0084}$, $b^2 = 0.054^{+0.011}_{-0.014}$ and $\zeta \leq 0.0445$ and for the third model $\Omega_D = 0.6947^{+0.0086}_{-0.0086}$, $b^2 = 0.0143^{+0.0032}_{-0.0054}$ and $\zeta \leq 0.0326$. Here we choose the scale factor at present time as $a_0 = 1$.

show the expected behavior of deceleration in the past and acceleration in the present time and future, in fact there is a transition from decelerating to accelerating phase at $z = 0.54$, $z = 0.51$ and $z = 0.48$ for models I, II and III respectively. Our results also show the phantom behavior of DE in the model I at late times. In the case of third model, w_D takes large negative values at very

Parameters	Best value	1σ	2σ
Ω_D	0.7009	± 0.0077	$^{+0.015}_{-0.016}$
ζ	0.116	$^{+0.044}_{-0.098}$	< 0.244
b^2	0.171	± 0.042	$^{+0.075}_{-0.078}$

TABLE VII: The best value of parameters and their uncertainty at 1σ and 2σ confidence levels for case I.

Parameters	Best value	1σ	2σ
Ω_D	0.695	± 0.0083	$^{+0.015}_{-0.016}$
ζ	0.035	< 0.0442	< 0.0930
b^2	0.053	$^{+0.011}_{-0.014}$	$^{+0.027}_{-0.024}$

TABLE VIII: Same as Tab(VII) but for case II

early times but it does not affect the model due to the negligible value of Ω_D at the early times. It is also notable that Ω_D of the first model takes non-zero values in the early universe. This is another difference of model I and models II and III.

For observational consistency check, we used Joint Light-curve analysis (JLA) for SNIa and used 59 Gamma-Ray Bursts data points as high redshift objects. Six observational indicators of BAO and 3 well-defined CMB parameters have been used for that purpose. For the first model, the joint analysis indicates that $\Omega_D = 0.7009^{+0.0077}_{-0.0077}$, $b^2 = 0.171^{+0.042}_{-0.042}$ and $\zeta = 0.116^{+0.044}_{-0.098}$ at 1 optimal variance error. For the second model the best fit values at 1σ confidence are $\Omega_D = 0.6961^{+0.0084}_{-0.0084}$, $b^2 = 0.054^{+0.011}_{-0.014}$ and $\zeta \leq 0.0445$. According to the combination of all observational data sets considered in this paper, the best fit values for third non-linear interacting dark energy model are $\Omega_D = 0.6947^{+0.0086}_{-0.0086}$, $b^2 = 0.0143^{+0.0032}_{-0.0054}$ and $\zeta \leq 0.0326$ at 1σ confidence interval. It is worth noting that the presence of interaction between dark sectors of the universe is confirmed at 4.10σ , 3.86σ and 2.65σ for models I, II and III respectively. Extending our approach to constraint on the models based on large scale structures and those observations beyond zero order perturbations could be interesting especially for discrimination between different models of interacting dark energy. This part of research is in progress and we will be addressing them later.

Parameters	Best value	1σ	2σ
Ω_D	0.6941	± 0.0086	$^{+0.018}_{-0.017}$
ζ	0.003	< 0.0341	< 0.0719
b^2	0.0147	$^{+0.0033}_{-0.0055}$	$^{+0.010}_{-0.0086}$

TABLE IX: Same as Tab(VII) but for case III

VI. ACKNOWLEDGMENT

The work of E. Ebrahimi has been supported by Research Institute for Astronomy and Astrophysics of Maragha, Iran.

-
- [1] A. G. Riess *et al.* [Supernova Search Team Collaboration], *Astron. J.* **116**, 1009 (1998).
 - [2] S. Perlmutter *et al.* [Supernova Cosmology Project Collaboration], *Astrophys. J.* **517**, 565 (1999).
 - [3] P. de Bernardis, *et al.*, *Nature* 404 (2000) 955.
 - [4] S. Perlmutter, *et al.*, *Astrophys. J.* 598 (2003) 102;
 - [5] S. Hanany *et al.*, *Astrophys. J. Lett.* 545, L5 (2000);
 - [6] C. B. Netterfield *et al.*, *Astrophys. J.* 571, 604 (2002);
 - [7] D.N. Spergel *et al.*, *Astrophys. J. Suppl.* 148, 175 (2003).
 - [8] P. A. R. Ade *et al.* [Planck Collaboration], arXiv:1502.01590 [astro-ph.CO].
 - [9] M. Colless *et al.*, *Mon. Not. R. Astron. Soc.* **328**, 1039 (2001);
 - [10] M. Tegmark *et al.*, *Phys. Rev. D* 69, 103501 (2004);
 - [11] S. Cole *et al.*, *Mon. Not. R. Astron. Soc.* **362**, 505 (2005);
 - [12] V. Springel, C.S. Frenk, and S.M.D. White, *Nature (London)* 440, 1137 (2006).
 - [13] W. J. Percival *et al.* [SDSS Collaboration], *Mon. Not. Roy. Astron. Soc.* **401**, 2148 (2010).
 - [14] C. Blake *et al.*, *Mon. Not. Roy. Astron. Soc.* **415**, 2876 (2011).
 - [15] B. A. Reid *et al.*, *Mon. Not. Roy. Astron. Soc.* **426**, 2719 (2012).
 - [16] V. Sahni and A. A. Starobinsky, *Int. J. Mod. Phys. D* **9**, 373 (2000).
 - [17] S. M. Carroll, *Living Rev. Rel.* **4**, 1 (2001).
 - [18] E. J. Copeland, M. Sami and S. Tsujikawa, *Int. J. Mod. Phys. D* **15**, 1753 (2006).
 - [19] A. De Felice and S. Tsujikawa, *Living Rev. Rel.* **13**, 3 (2010).
 - [20] S. Tsujikawa, *Lect. Notes Phys.* **800**, 99 (2010).
 - [21] T. Clifton, P. G. Ferreira, A. Padilla and C. Skordis, *Phys. Rept.* **513**, 1 (2012).
 - [22] Amendola, L., Appleby, S., Bacon, D., *et al.*, *Cosmology and fundamental physics with the Euclid satellite*. 2012a, ArXiv e-prints, arXiv:1206.1225
 - [23] J. Sola and H. Stefancic, *Phys. Lett. B* 624, 147 (2005).
 - [24] C. Wetterich, *Nucl. Phys. B* 302 (1988) 668;
 - [25] B. Ratra, J. Peebles, *Phys. Rev. D* 37 (1988) 321.
 - [26] S. Dutta, E. N. Saridakis and R. J. Scherrer, *Phys. Rev. D* 79, 103005 (2009).
 - [27] E. N. Saridakis and S. V. Sushkov, *Phys. Rev. D* 81, 083510 (2010).
 - [28] S. Rahvar and M. S. Movahed, *Phys. Rev. D* **75**, 023512 (2007).
 - [29] R. R. Caldwell, *Phys. Lett. B* 545, 23 (2002).

- [30] S. Nojiri and S. D. Odintsov, Phys. Lett. B 562, 147 (2003)
- [31] P. Singh, M. Sami and N. Dadhich, Phys. Rev. D 68, 023522 (2003).
- [32] W. Hu, Phys. Rev. D 71, 047301 (2005).
- [33] M. R. Setare and E. N. Saridakis, JCAP 0903, 002 (2009).
- [34] E. N. Saridakis, Nucl. Phys. B 819, 116 (2009).
- [35] S. D. H. Hsu, Phys. Lett. B 594, 13 (2004).
- [36] M. Li, Phys. Lett. B 603, 1 (2004).
- [37] Q. G. Huang and M. Li, JCAP 0408, 013 (2004).
- [38] E. Elizalde, S. Nojiri, S. D. Odintsov and P. Wang, Phys. Rev. D 71, 103504 (2005)
- [39] E. N. Saridakis, Phys. Lett. B 660, 138 (2008)
- [40] E. N. Saridakis, JCAP 0804, 020 (2008).
- [41] R.G. Cai, Phys. Lett. B 657, 228 (2007).
- [42] H. Wei and R.G. Cai, Phys. Lett. B 660, 113 (2008).
- [43] H. Wei and R.G. Cai, Eur. Phys. J. C 59, 99 (2009)
- [44] K. Bamba, S. Capozziello, S. Nojiri and S. D. Odintsov, arXiv:1205.3421v3.
- [45] F. R. Urban and A. R. Zhitnitsky, Phys. Lett. B 688 (2010) 9 ;Phys. Rev. D 80 (2009) 063001; JCAP 0909 (2009) 018; Nucl. Phys. B 835 (2010) 135.
- [46] N. Ohta, Phys. Lett. B 695 (2011) 41, arXiv:1010.1339.
- [47] K. Kawarabayashi and N. Ohta, Nucl. Phys. B 175, 477 (1980).
- [48] E. Witten, Nucl. Phys. B 156 (1979) 269;
- [49] G. Veneziano, Nucl. Phys. B 159 (1979) 213.
- [50] C. Rosenzweig, J. Schechter and C. G. Trahern, Phys. Rev. D 21 (1980) 3388.
- [51] P. Nath and R. L. Arnowitt, Phys. Rev. D 23 (1981) 473.
- [52] R.G. Cai, Z.L. Tuo, H.B. Zhang, arXiv:1011.3212.
- [53] A. Sheykhi, A. Bagheri, Europhys. Lett. 95, 39001 (2011).
- [54] E. Ebrahimi, A. Sheykhi, Phys. Lett. B 705, 19 (2011).
- [55] E. Ebrahimi, A. Sheykhi, Int. J. Mod. Phys. D 20, 2369 (2011)
- [56] A. Sheykhi, M. Sadegh Movahed , General Relativity and Gravitation, Volume 44, Issue 2, 449-465 (2012).
- [57] Chao-Jun Feng, Xin-Zhou Li, Ping Xi, JHEP 1205(2012) 046.
- [58] Chao-Jun Feng, Xin-Zhou Li, Xian-Yong Shen, Phys.Rev. D87 (2013) 023006.
- [59] Chao-Jun Feng, Xin-Zhou Li, Xian-Yong Shen, Mod. Phys. Lett. A27 (2012) 1250182.
- [60] R. G. Cai, Z. L. Tuo, Y. B. Wu, Y. Y. Zhao, Phys. Rev. D 86 (2012) 023511.
- [61] E. Ebrahimi, A. Sheykhi and H. Alavirad, Central Eur. J. Phys. 11, no. 7, 949 (2013).
- [62] Bertolami O, Gil Pedro F and Le Delliou M 2007 Phys. Lett. B 654 165.
- [63] G. Olivares, F. Atrio, D. Pavon, Phys. Rev. D 71 (2005) 063523.
- [64] Jian-Hua He and Bin Wang, JCAP 0806, 010 (2008).

- [65] E. Ebrahimi, A. Sheykhi, *Int J Theor Phys* (2013) 52:29661776.
- [66] F. Arevalo, A. P. R. Bacalhau and W. Zimdahl, *Class. Quant. Grav.* **29**, 235001 (2012)
- [67] G. Hinshaw *et al.* [WMAP Collaboration], *Astrophys. J. Suppl.* **208**, 19 (2013)
- [68] P. A. R. Ade *et al.* [Planck Collaboration], arXiv:1502.01589 [astro-ph.CO].
- [69] Suzuki, N., *et al.* 2012, *ApJ*, 746, 85
- [70] S. Cao and Z. H. Zhu, *Phys. Rev. D* **90**, no. 8, 083006 (2014)
- [71] <http://supernova.lbl.gov/Union/>
- [72] Li, Z. X., Wu, P. X., & Yu, H. W. 2011, *PLB*, 695, 1
- [73] Schaefer, B. E. 2003, *ApJ*, 583, L67
- [74] Schaefer, B. E. 2007, *ApJ*, 660, 16
- [75] Wright, E. L. 2007, *ApJ*, 664, 633
- [76] Amati, L., *et al.* 2008, *MNRAS*, 391, 577b
- [77] Daly, R. A., *et al.* 2008, *ApJ*, 677, 1
- [78] Di Pietro, E., & Claeskens, J. F. 2003, *MNRAS*, 341, 1299
- [79] Padmanabhan, N., *et al.*, *Mon. Not. Roy. Astron. Soc.* **427**, 2132 (2012).
- [80] Anderson, L., *et al.*, *Mon. Not. Roy. Astron. Soc.* **427**, 3435 (2013).
- [81] Blake, C., *et al.* 2012, *MNRAS*, 425, 405
- [82] Beutler, F., *et al.* 2011, *MNRAS*, 416, 3017
- [83] C. Blake *et al.*, *Mon. Not. Roy. Astron. Soc.* **418**, 1707 (2011)
- [84] Hu, W., & Sugiyama, N. 1996, *ApJ*, 471, 542
- [85] H. Akaike, A new look at the statistical model identification, *IEEE Trans. Automatic Control* 19, 716 (1974).
- [86] G. Schwarz, Estimating the dimension of a model. *Ann. Stat.* 6, 461 (1978)
- [87] Y. Y. Xu and X. Zhang, arXiv:1607.06262 [astro-ph.CO].